Asociación Argentina
de Mecánica Computacional

Mecánica Computacional Vol XXXII, págs. 1259-1270 (artículo completo)
Carlos G. García Garino, Aníbal E. Mirasso, Mario A. Storti, Miguel E. Tornello (Eds.)
Mendoza, Argentina, 19-22 Noviembre 2013

NUMERICAL SIMULATION IN UNCONVENTIONAL RESERVOIRS

Lucas A. Macias[a], Gabriela B. Savioli[a] and Juan E. Santos[b]

[a]*Laboratorio de Ingeniería de Reservorios, Instituto del Gas y del Petróleo, Facultad de Ingeniería, Universidad de Buenos Aires, Av. Las Heras 2214 Piso 3 C1127AAR Buenos Aires, Argentina, gsavioli@fi.uba.ar*

[b]*CONICET, Instituto del Gas y del Petróleo, Facultad de Ingeniería, Universidad de Buenos Aires and, Universidad de La Plata and, Department of Mathematics, Purdue University, 150 N. University Street, West Lafayette, Indiana, 47907-2067, USA, santos@math.purdue.edu*

Keywords: unconventional reservoirs, hydraulic fractures, seismic monitoring

Abstract. Non conventional hydrocarbon reservoirs are characterized by their very low permeability and porosity. To allow oil and gas production, the reservoir has to be fractured using different techniques, like fluid injection at high pressures from a well drilled in the formation (fracking). The final goal is to create a fracture network that combines existing natural fractures with the new generated ones. The changes in permeability and porosity in the saturated porous media due to the fracking procedure will induce changes in the seismic response. The objective of this work is the numerical modeling of multiphase flow and seismic wave propagation in unconventional reservoirs. The multiphase flow through porous media is described by the well-known Black-Oil formulation, which uses as a simplified thermodynamic model, the PVT data: formation volumen factors and gas solubility in oil and water. The numerical solution is obtained using an IMPES (IMplicit Pressure Explicit Saturation) finite difference technique. The propagation of waves in fluid-saturated porous media is described using a viscoelastic model that takes into account the dispersion and attenuation effects due to the presence of heterogeneities in the fluid and solid phase properties. This model is numerically solved applying an iterative finite element domain decomposition procedure. As an example, we analyze a tight gas reservoir. The results of the simulations show the capability of the seismic techniques to detect the presence of fractures.

1 INTRODUCTION

The process of hydraulic fracturing consists in injecting fluids at high pressure into a reservoir in order to produce fractures or to connect existing natural fractures thus creating a pathway by which the hydrocarbons can flow to the wellbore (Riahi and Damjanac, 2013). This technique allows to enhance the fluid flow from the formation to the wellbore and consequently the oil or gas production. When it comes to unconventional reservoirs (tight or shale), this technique turns out to be indispensable for the well to become productive (Nagel et al., 2013).

Numerical modeling of water injection, fracture generation and seismic monitoring are important tools to understand the hydraulic fracturing process and to determine its characteristics and the main variables to consider. To perform this task properly, a reliable geological model of the shale formation is important, which simulates the geometry and petroelastical properties. The model applied in this work assumes a shaly sand depending on the clay content. The permeability is assumed to be anisotropic and is obtained from first principles as a function of porosity and grain sizes. Besides, the model takes into account the variation of properties with pore pressure and fluid saturation (Carcione et al., 2006).

Rigorous modeling of hydraulic fracturing can be seen in Wangen (2011), based on Biot's equation and a finite element representation of the fracture pressure; and also in (Pak and Chan, 2008), where a fully coupled thermal hydro-mechanical model is developed. In this work we select a simplified approach to simulate fluid injection and fracture generation: we apply the well known Black-Oil formulation to simulate the simultaneous flow of water and gas in our unconventional reservoir (Aziz and Settari, 1985; Fanchi, 1997). The simulator is run through different stages: as reservoir pressure increases and exceeds a limit value, petrophysical properties are updated and a new run begins. The fluid pressures and saturations computed by the fluid simulator are used to obtain the properties of the gas and water at in-situ conditions and the petrophysical properties of the formation (Carcione, 2007).

The changes in permeability and porosity due to the fracking procedure and the presence of injected fluids will change the seismic response (Sena et al., 2011). Our wave propagation simulator is based on a viscoelastic model that considers dispersion and attenuation effects. In regions with partial gas saturation, following White's theory (White et al., 1975), we consider P-wave attenuation due to wave-induced fluid flow at mesoscopic scales using a model of porous layers alternately saturated with water and gas. An iterative finite element domain decomposition procedure is applied to solve the differential equations (Santos et al., 2008).

This work presents the simulations of water injection, fracture generation and time-lapse seismograms in an unconventional gas reservoir with low permeability and porosity. The proposed methodology allows us to simulate a hydraulic fracture and its detection through seismic monitoring.

2 THE BLACK-OIL FORMULATION OF TWO-PHASE FLOW IN POROUS MEDIA

The simultaneous flow of water and gas in porous media is described by the well-known Black-Oil formulation applied to two-phase, two component fluid flow (Aziz and Settari, 1985). In this way, gas component may dissolve in the water phase but the water is not allowed to vaporize into the gas phase. The differential equations, obtained by combining the mass conservation equations with Darcy's empirical law, are

$$\nabla \cdot \left(\underline{\kappa} \left(\frac{k_{rg}}{B_g \eta_g} (\nabla p_g - \rho_g g \nabla D) + \frac{R_s k_{rw}}{B_w \eta_w} (\nabla p_w - \rho_w g \nabla D) \right) \right) + \frac{q_g}{\rho_g^{SC}} = \frac{\partial \left[\phi \left(\frac{S_g}{B_g} + \frac{R_s S_w}{B_w} \right) \right]}{\partial t}, \tag{1}$$

$$\nabla \cdot \left(\underline{\kappa} \frac{k_{rw}}{B_w \eta_w} (\nabla p_w - \rho_w g \nabla D) \right) + \frac{q_w}{\rho_w^{SC}} = \frac{\partial \left[\phi \frac{S_w}{B_w} \right]}{\partial t}, \tag{2}$$

where g, w denote water and gas phases, respectively. The unknowns for the Black-Oil model are the fluid pressures p_β and saturations S_β ($\beta = w, g$). Also ρ_β is density, q_β injection mass rate per unit volume, $k_{r\beta}$ relative permeability and η_β viscosity. Finally ϕ is porosity and $\underline{\kappa}$ is the absolute permeability tensor in 2D,

$$\underline{\kappa} = \begin{pmatrix} \kappa_x & 0 \\ 0 & \kappa_z \end{pmatrix} \tag{3}$$

Two algebraic equations relating the saturations and pressures complete the system:

$$S_w + S_g = 1, \qquad p_g - p_w = P_C(S_w), \tag{4}$$

where P_C is the capillary pressure.

The Black-Oil formulation uses as a simplified thermodynamic model, the PVT data defined as

- R_s: gas solubility in water;
- B_g: gas formation volume factor;
- B_w: water formation volume factor;

The conversion of compositional data from equations of state into the Black-Oil PVT data is performed applying an algorithm developed by Hassanzadeh et al. (2008),

- $R_s = \dfrac{\tilde{\rho}_w^{SC} \chi_g}{\tilde{\rho}_g^{SC} (1 - \chi_g)}$
- $B_w = \dfrac{\rho_w^{SC}}{\rho_w (1 - \omega_g)}$,

where, ρ_w^{SC} and ρ_g^{SC} are the water and gas molar densities at standard conditions and χ_g and ω_g are the gas mole and mass fraction in the water phase.

The numerical solution was obtained employing the public domain software BOAST (Fanchi, 1997). BOAST solves the differential equations using IMPES (IMplicit Pressure Explicit Saturation), a finite difference technique (Aziz and Settari, 1985). Finite differences is the standard

in commercial reservoir simulators, and the improved versions use both structured and unstructured grids with local refinements to accurately represent reservoir geometry. The basic idea of IMPES is to obtain a single pressure equation by a combination of the flow equations. Once pressure is implicitly computed for the new time, saturation is updated explicitly. We briefly describe IMPES for these particular system (1), (2), (4). The first step is to obtain the pressure equation, combining flow equations: Eq. (1) multiplied by B_g and Eq.(2) multiplied by $(B_w - R_s B_g)$ are added. In this way, the right side of the resulting equation is:

$$B_g \frac{\partial \left[\phi \left(\frac{S_g}{B_g} + \frac{R_s S_w}{B_w} \right) \right]}{\partial t} + (B_w - R_s B_g) \frac{\partial \left[\phi \frac{S_w}{B_w} \right]}{\partial t}$$

Using the chain rule to expand the time derivatives and after some computations and rearrangements, the right side becomes:

$$\phi \left[\frac{1}{\phi} \frac{d\phi}{dp_w} + S_g \left(-\frac{1}{B_g} \frac{dB_g}{dp_w} \right) + S_w \left(-\frac{1}{B_w} \frac{dB_w}{dp_w} + \frac{B_g}{B_w} \frac{dR_s}{dp_w} \right) \right] \frac{\partial p_w}{\partial t},$$

where all time derivatives of saturation disappear.

Defining the following aproximate compressibilities,

- Formation compressibility: $c_f = \dfrac{1}{\phi} \dfrac{d\phi}{dp_w}$
- Gas compressibility: $c_g = -\dfrac{1}{B_g} \dfrac{dB_g}{dp_w}$,
- Brine compressibility: $c_w = -\dfrac{1}{B_w} \dfrac{dB_w}{dp_w} + \dfrac{B_g}{B_w} \dfrac{dR_s}{dp_w}$,
- Total compressibility: $c_t = c_f + S_g c_g + S_w c_w$,

the right side is simply expressed as,

$$\phi c_t \frac{\partial p_w}{\partial t}.$$

Finally, replacing p_g by $p_w + P_C(S_w)$ in the left side of the combined equation, the following pressure equation in p_w is obtained,

$$\begin{aligned} & B_g \left[\nabla \cdot \left(\underline{\kappa} \left(\frac{k_{rg}}{B_g \eta_g} (\nabla p_w - \rho_g g \nabla D) + \frac{R_s k_{rw}}{B_w \eta_w} (\nabla p_w - \rho_w g \nabla D) + \frac{k_{rg}}{B_g \eta_g} \nabla P_C \right) \right) \right] \\ & + (B_w - R_s B_g) \left[\nabla \cdot \left(\underline{\kappa} \frac{k_{rw}}{B_w \eta_w} (\nabla p_w - \rho_w g \nabla D) \right) \right] \\ & + B_g \frac{q_g}{\rho_g^{SC}} + (B_w - R_s B_g) \frac{q_w}{\rho_w^{SC}} = \phi c_t \frac{\partial p_w}{\partial t}. \end{aligned} \tag{5}$$

In BOAST simulator, system (2) , (5) is discretized using a block centered grid. The system is linearized evaluating the pressure and saturation dependent funcions (PVT parameters, viscosities, relative permeabilities and capillary pressure) in the pressure and saturation values

of the previous time step. The pressure equation is solved implicitly, applying a Block Successive Over Relaxation method (BSOR) to compute the linear system solution. The saturation equation is solved explicitly, therefore stability restrictions are considered to select the time step (Savioli and Bidner, 2005).

3 A VISCOELASTIC MODEL FOR WAVE PROPAGATION

The propagation of waves in a fluid-saturated porous media is described using a viscoelastic model that takes into account the dispersion and attenuation effects due to the presence of heterogeneities in the fluid and solid phase properties (mesoscopic-scale heterogeneities).

The equation of motion in a 2D isotropic viscoelastic domain Ω with boundary $\partial\Omega$ can be stated in the space-frequency domain as

$$-\omega^2\rho u - \nabla\cdot\sigma(u) = f(x,\omega), \quad \Omega \tag{6}$$

$$-\sigma(u)\nu = i\omega\mathcal{D}u, \quad \partial\Omega, \tag{7}$$

where $u=(u_x,u_y)$ is the displacement vector. Here ρ is the bulk density and (7) is a first-order absorbing boundary condition using the positive definite matrix $\mathcal{D}$, which definition is given in (Ha et al., 2002).

The stress tensor $\sigma(u)$ is defined in the space-frequency domain by

$$\sigma_{jk}(u) = \lambda_G(\omega)\nabla\cdot u\delta_{jk} + 2\mu(\omega)\varepsilon_{jk}(u), \quad \Omega, \tag{8}$$

where $\varepsilon_{jk}(u)$ denotes the strain tensor and δ_{jk} is the Kroenecker delta.

The coefficient μ in (8) is the shear modulus of the dry matrix, while the Lamé coefficient is $\lambda_G = K_G - \mu$ in 2D. K_G is the Gassmann's undrained bulk modulus, computed as follows:

$$K_G = K_m + \alpha^2 K_{av}$$

$$\alpha = 1 - \frac{K_m}{K_s},$$

$$K_{av} = \left[\frac{\alpha-\phi}{K_s} + \frac{\phi}{K_f}\right]^{-1}.$$

where

- K_m: bulk modulus of the dry matrix
- K_s: bulk modulus of the solid grains
- K_f: bulk modulus of the saturant fluid

These viscoelastic model assumes an effective single-phase fluid. Therefore, the effective fluid density, viscosity and bulk modulus are obtained using the properties of the gas and brine weighted by the corresponding saturations computed by the BOAST flow simulator. Following White et al. (1975), we consider P-wave attenuation due to wave induced fluid flow at mesoscopic scale using a model of porous layers alternately saturated with water and gas respectively. At this step, the spatial saturation distribution computed by BOAST is used to determine the phase velocities and attenuation coeficients of P and S waves from White's model. This approach yields a complex and frequency dependent P-wave modulus $E(\omega) = \lambda_G(\omega) + 2\mu(\omega)$

for the formation. Recall that in a viscoelastic solid, the phase velocity and quality factor $Q(\omega)$ are defined by the relations

$$v_p(\omega) = \left[\mathrm{Re}\left(\frac{1}{vc_p(\omega)}\right)\right]^{-1}, \qquad Q(\omega) = \frac{\mathrm{Re}(vc_p(\omega)^2)}{\mathrm{Im}(vc_p(\omega)^2)}, \tag{9}$$

where $vc_p(\omega)$ is the complex and frequency dependent compressional velocity defined as

$$vc_p(\omega) = \sqrt{\frac{E(\omega)}{\rho}}. \tag{10}$$

S-wave attenuation is also taken into account making the shear modulus complex and frequency dependent using another relaxation mechanism related to the P-wave mechanism (Carcione et al., 2012).

The approximate solution of (6) with the boundary conditions (7) is obtained using an iterative finite element domain decomposition procedure (Santos et al., 2008).

4 UNCONVENTIONAL GAS RESERVOIR MODEL

We consider a 2D unconventional gas reservoir of $200m$ thickness and $500m$ length located at $2500m$ depth, which is modeled with a $1m$ x $1m$ cell grid. The formation rock is a shaly sand with very high clay content $C = 90\%$ and low initial porosity $\phi_0 = 0.2$. The other petrophysical properties are obtained from initial porosity and clay content using the model described in the next seccion (Carcione et al., 2006). The reservoir is considered isothermal with initial gas saturation of 90%. The initial pressure p_H is computed using equilibrium conditions. Gas properties (viscosity, density and bulk modulus) are obtained from the Peng-Robinson equations as a function of temperature and pore pressure p.

5 SIMULATION OF WATER INJECTION AND FRACTURE PROPAGATION

To allow gas production, the reservoir is fractured injecting water at a constant flow rate of $0.11m^3/s$. The injection point is located $135m$ beneath the formation top and centered in the x direction.

Water injection is modeled applying the BOAST Simulator. In order to simulate fracture propagation, we apply a criterion based on a "breakdown pressure", which is computed from the horizontal stresses and the tensile stress of the rock (Economides and Hill, 1994). The criterion is defined as follows: once pore pressure p becomes greater than breakdown pressure on a certain grid cell, this cell is "fractured", i.e. the cell clay content is strongly reduced. When this happens, we update the cell porosity applying the following equation that relates this property with pore pressure (Carcione et al., 2006),

$$\frac{(1-\phi_c)}{K_s}(p(t) - p_H) = \phi_0 - \phi(t) + \phi_c \ln\frac{\phi(t)}{\phi_0}. \tag{11}$$

where ϕ_c is a critical porosity and K_s the bulk modulus of the solid grain, which is the arithmetic average of the Hashin-Shtrikman upper and lower bounds.

Once porosity is computed, the other petrophysical properties are also updated using the pressures and saturations values obtained by BOAST. Horizontal permeability κ_x is computed

as (Carcione et al., 2006),

$$\frac{1}{\kappa_x(t)} = \frac{45(1-\phi(t))^2}{\phi(t)^3}\left(\frac{(1-C(t))^2}{R_q^2} + \frac{C(t)^2}{R_c^2}\right) \tag{12}$$

considering average radii of sand ($R_q = 50\mu m$) and clay ($R_c = 1.5\mu m$) particles. Besides, vertical permeability is obtained from horizontal permeability and water saturation as,

$$\frac{\kappa_x(t)}{\kappa_z(t)} = \frac{1-(1-0.3a)\sin\pi S_w(t)}{a(1-0.5\sin\pi S_w(t))} \tag{13}$$

using an anisotropy factor $a = 0.1$.

Summarizing, these model use a two-time step procedure: 1) the breakdown pressure verification and the resulting petrophysical properties update is performed each $\delta T = 600s$; 2) during each time period δT, pressure and saturations distributions are computed by BOAST simulator using constant petrophysical properties and a time increment $\delta t = 5s$.

Figure 1, 2 and 3 show the horizontal permeability (κ_x), pore pressure (p) and water saturation (S_w) maps obtained after 5 hours of water injection using the procedure described above. These pictures allow us to see the fractured zone and also the pressure and water distribution. These local properties and fluid changes will be use to detect the fracture using seismic monitoring.

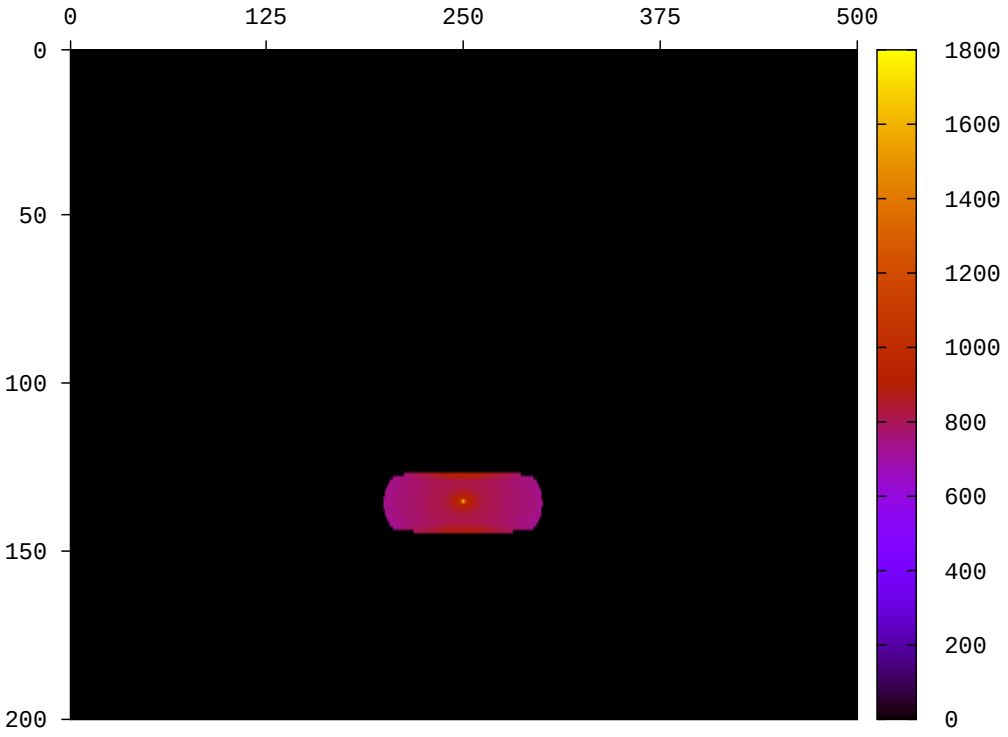

Figure 1: Horizontal permeability map after fracking (mDa)

6 TIME-LAPSE SEISMIC MONITORING

To analyze the capability of seismic monitoring to identify fractured zones, we use the BOAST results to determine the geophysical properties needed to run the seismic model. Poros-

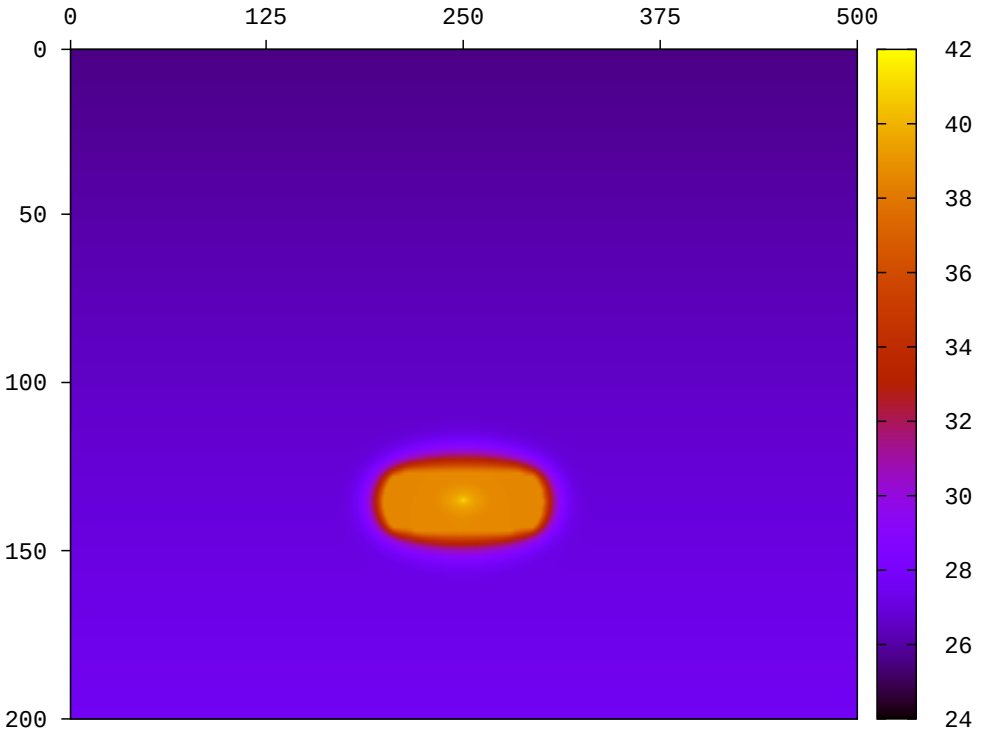

Figure 2: Pore pressure map after fracking (MPa)

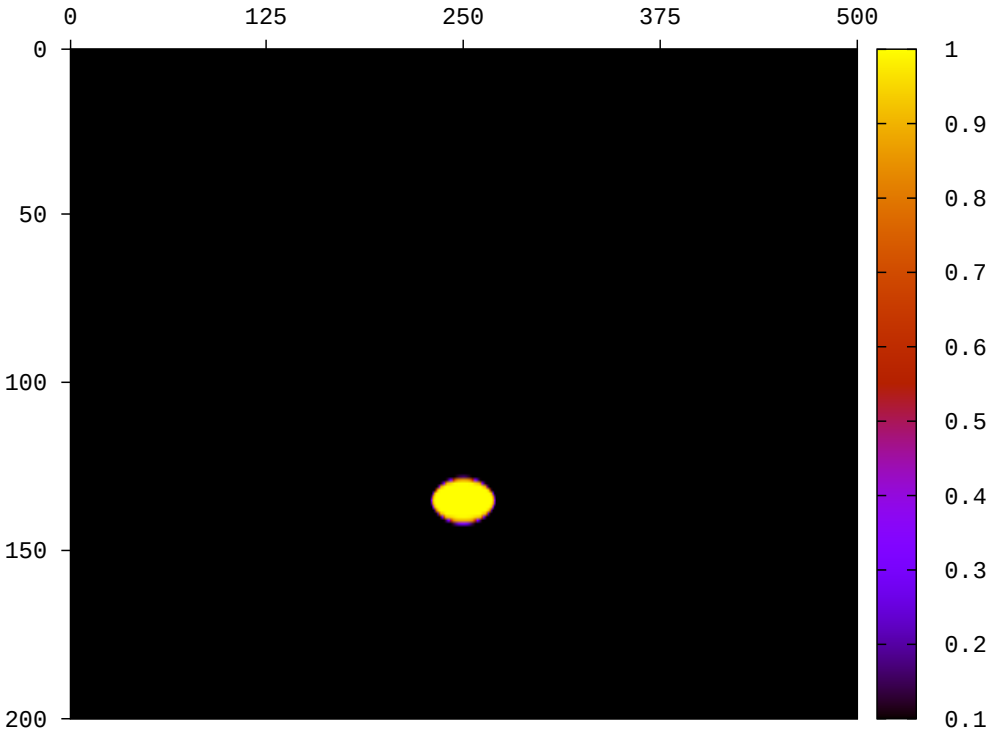

Figure 3: Water saturation map after fracking

ity, horizontal permeability and vertical permeability are updated as described in the previous section, using pressure and saturation distributions computed by BOAST. Besides, the bulk and shear moduli of the dry matrix are computed using the Krief model, that depends on porosity (Carcione et al., 2006). Then the media is excited with a line of punctual sources along the surface with central frequency $90Hz$ and highest frequency $180Hz$. The distance between each source is $12m$. The viscoelastic wave equation is solved for 200 frequencies, and the time histories were obtained using an approximate inverse Fourier transform. Figure 4, displays P-wave phase velocity v_p after the fracking procedure showing the influence of fracture permeability and water saturation in the velocity increment. Time histories measured near the surface are shown in Figure 5 before (left) and after (right) fracking, respectively. The reflection in Figure 5 (right) is due to the presence of the fracture in the formation.

Finally, Figure 6 shows snapshots of vertical component of the solid phase velocity at 30, 70, 90 and $110ms$ after fracking. At $70ms$ (Figure 6b) the waves generated by the line source are arriving at the fracture. At $90ms$ (Figure 6c) and $110ms$ (Figure 6d) the waves reflected and transmitted from the fracture are clearly observed.

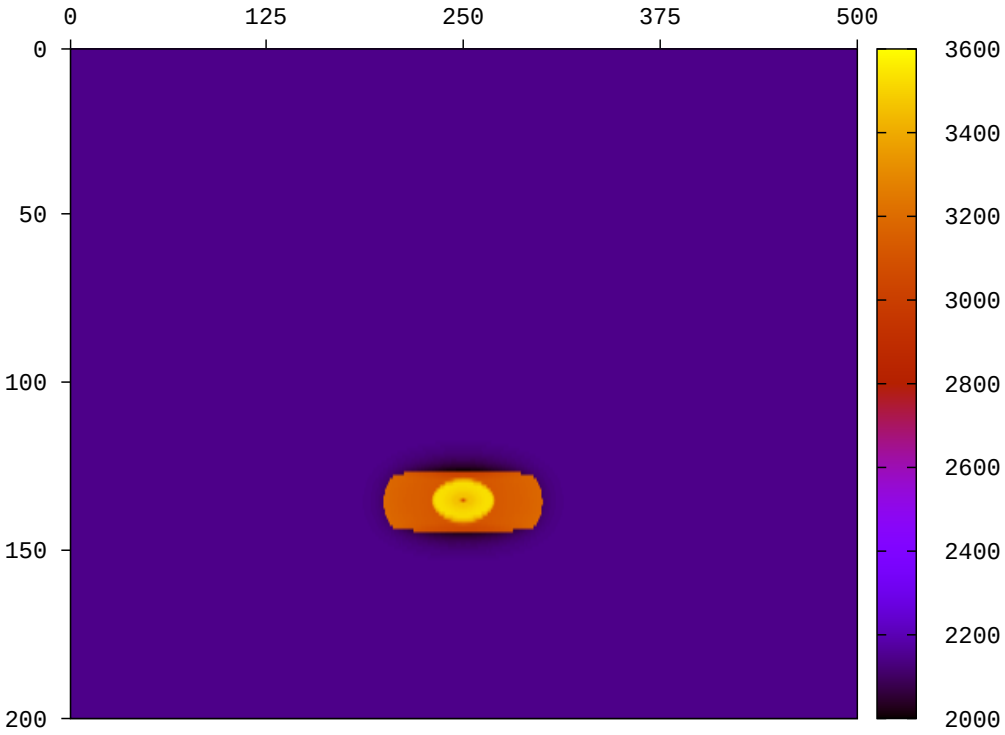

Figure 4: P-wave phase velocity map after fracking

7 CONCLUSIONS

In this work, a numerical approach is used to simulate fracture propagation: we apply a black oil simulator to model fluid injection and a "breakdown pressure" criterion to determine the cells to be fractured. The petrophysical properties of fractured cells are updated assuming an abrupt descent of clay content and using the model described by Carcione. Applying a seismic wave propagation simulator, the changes in the sesmic response due to permeability, porosity and fluid saturation variation after the fracking procedure are clearly observed. The seismic

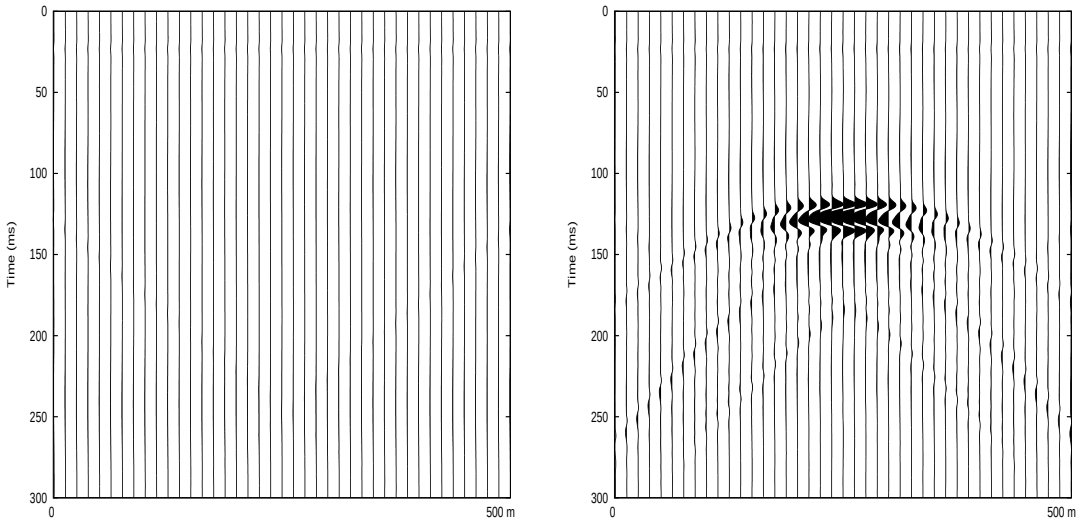

Figure 5: Traces of the vertical component of the velocity before (left) and after (right) fracking procedure

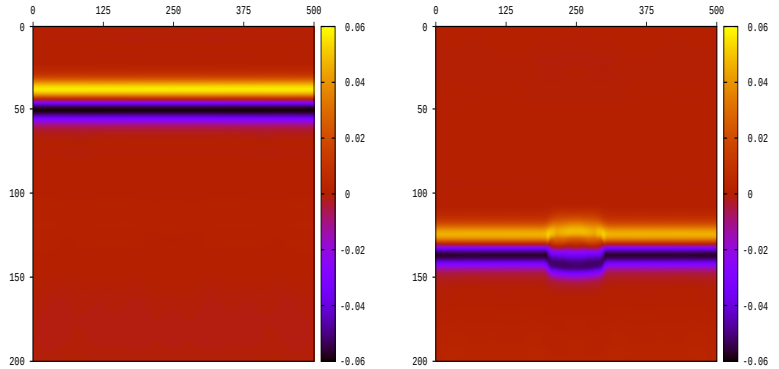

(a) $30ms$ (b) $70ms$

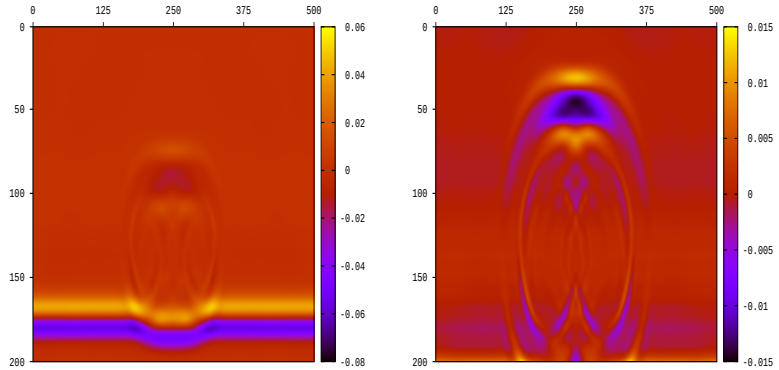

(c) $90ms$ (d) $110ms$

Figure 6: Snapshots of vertical component of the solid phase velocity at different times

model includes attenuation and dispersion effects due to mesoscopic scale heterogeneities using White's theory. The numerical examples show the effectiveness of combining multiphase flow simulators in porous media with seismic monitoring to detect the presence of fractures in an unconventional gas reservoir with low permeability and porosity.

8 AKNOWLEDGEMENTS

This work was partially funded by CONICET, Argentina (PIP 0952), Universidad de Buenos Aires (UBACyT 20020120100270) and Peruilh grant provided by Facultad de Ingeniería - Universidad de Buenos Aires.

REFERENCES

Aziz K. and Settari A. *Petroleum Reservoir Simulation*. Elsevier Applied Science Publishers, Great Britain, 1985.

Carcione J., Gei D., Picotti S., and Michelini A. Cross-hole electromagnetic and seismic modeling for co2 and monitoring in a saline aquifer. *Journal of Petroleum Science and Engineering*, 2012. In press.

Carcione J.M. *Wave fields in real media: Wave propagation in anisotropic, anelastic, porous and electromagnetic media*, volume 38 of *Handbook of Geophysical Exploration*. Elsevier, 2nd edition, revised and extended, 2007.

Carcione J.M., Picotti S., Gei D., and Rossi G. Physics and seismic modeling for monitoring CO_2 storage. *Pure and Applied Geophysics*, 163:175–207, 2006.

Economides M.J. and Hill A.D. *Petroleum Production Systems*. Prentice Hall PTR, New Jersey, USA, 1994.

Fanchi J. *Principles of Applied Reservoir Simulation*. Gulf Professional Publishing Company, Houston, Texas, 1997.

Ha T., Santos J.E., and Sheen D. Nonconforming finite element methods for the simulation of waves in viscoelastic solids. *Comput. Meth. Appl. Mech. Engrg.*, 191:5647–5670, 2002.

Hassanzadeh H., Pooladi-Darvish M., Elsharkawy A., Keith D., and Leonenko Y. Predicting PVT data for CO_2-brine mixtures for black-oil simulation of CO_2 geological storage. *International Journal of Greenhouse Gas Control*, 2:65–77, 2008.

Nagel N., Zhang F., Sanchez-Nagel M., and Lee B. Numerical study of interaction between hydraulic fracture and discrete fracture network. In A. Bunger, J. McLennan, and R. Jeffrey, editors, *Quantitative Evaluation of Completion Techniques on Influencing Shale Fracture âĂŸComplexityâĂŹ*. INTECH, 2013.

Pak A. and Chan D. Numerical modeling of hydraulic fracturing in oil sands. *Scientia Iranica*, 15:516–535, 2008.

Riahi A. and Damjanac B. Numerical study of interaction between hydraulic fracture and discrete fracture network. In A. Bunger, J. McLennan, and R. Jeffrey, editors, *Effective and Sustainable Hydraulic Fracturing*. INTECH, 2013.

Santos J., Rubino J., and Ravazzoli C. Modeling mesoscopic attenuation in highly heterogeneus biot's medium employing an equivalent viscoelastic model. *Proc. 78th Annual International Meeting SEG*, pages 2212–2215, 2008.

Savioli G. and Bidner M.S. Simulation of the oil and gas flow toward a well - a stability analysis. *Journal of Petroleum Science and Engineering*, 48:53–69, 2005.

Sena A., Castillo G., Chesser K., Voisey S., Estrada J., Carcuz J., Carmona E., and Hodgkins P. Seismic reservoir characterization in resource shale plays: Stress analysis and sweet spot discrimination. *The Leading Edge*, pages 758–764, 2011.

Wangen M. Finite element modeling of hydraulic fracturing on a reservoir scale in 2d. *Journal of Petroleum Science and Engineering*, pages 274–285, 2011.

White J.E., Mikhaylova N.G., and Lyakhovitskiy F.M. Low-frequency seismic waves in fluid-saturated layered rocks. *Izvestija Academy of Siences USSR, Physics of Solid Earth*, 10:654–659, 1975.